HHS Public Access

Author manuscript

Neurobiol Dis. Author manuscript; available in PMC 2018 July 01.

Published in final edited form as:

Neurobiol Dis. 2017 July ; 103: 174–183. doi:10.1016/j.nbd.2017.04.013.

Loss of the neurodevelopmental gene Zswim6 alters striatal morphology and motor regulation

David J. Tischfield[a,b], **Dave K. Saraswat**[b], **Andrew Furash**[c], **Stephen C. Fowler**[d], **Marc V. Fuccillo**[c], and **Stewart A. Anderson**[a,b]

[a]Neuroscience Graduate Group, Perelman School of Medicine, University of Pennsylvania, Philadelphia, PA 19104-6085, USA

[b]Department of Psychiatry, Children's Hospital of Philadelphia, University of Pennsylvania School of Medicine ARC 517, Philadelphia, PA 19104-5127, USA

[c]Department of Neuroscience, Perelman School of Medicine, University of Pennsylvania, Philadelphia, PA 19104-6085, USA

[d]Department of Pharmacology and Toxicology, University of Kansas, Lawrence, KS 66045, USA

Abstract

The zinc-finger SWIM domain-containing protein 6 (ZSWIM6) is a protein of unknown function that has been associated with schizophrenia and limited educational attainment by three independent genome-wide association studies. Additionally, a putatively causal point mutation in ZSWIM6 has been identified in several cases of acromelic frontonasal dysostosis with severe intellectual disability. Despite the growing number of studies implicating ZSWIM6 as an important regulator of brain development, its role in this process has never been examined. Here, we report the generation of Zswim6 knockout mice and provide a detailed anatomical and behavioral characterization of the resulting phenotype. We show that Zswim6 is initially expressed widely during embryonic brain development but becomes restricted to the striatum postnatally. Loss of Zswim6 causes a reduction in striatal volume and changes in medium spiny neuron morphology. These changes are associated with alterations in motor control, including hyperactivity, impaired rotarod performance, repetitive movements, and behavioral hyperresponsiveness to amphetamine. Together, our results show that Zswim6 is indispensable to normal brain function and support the notion that Zswim6 might serve as an important contributor to the pathogenesis of schizophrenia and other neurodevelopmental disorders.

*Correspondence should be addressed to S.A.A (sande@mail.med.upenn.edu).

Author Contributions

D.J.T and S.A.A generated the Zswim6 KO mouse line. D.J.T performed qPCR, ISH, IHC, and animal breeding. D.J.T and D.K.S. performed cell counting and cell tracings. D.J.T, A.F, S.C.F, and M.V.F performed and analyzed behavioral experiments. D.J.T, S.A.A, M.V.F, and S.C.F wrote the manuscript.

Keywords

ZSWIM6; striatum; schizophrenia; medium spiny neurons; hyperactivity; motor behavior; neurodevelopment

INTRODUCTION

While neuropsychiatric disorders such as schizophrenia (SCZ) exhibit significant heritability, the underlying genetics are complex, involving multiple perturbations of modest effect size acting within critical temporal windows[1]. Efforts to understand the pathophysiology of SCZ are similarly complicated by the disorder's diverse symptomology, organized loosely around positive (hallucinations and delusions) and negative (altered affect, reduced pleasure and motivation) symptom domains. However, after years of painstaking progress, advances in genomic sequencing have started to uncover the genetic building blocks of polygenic disorders such as SCZ. While knockout animal models generally oversimplify the complex nature of these disorders, they can be useful in identifying molecular pathways and neural circuits that are vulnerable to genetic insult and that have central functions in regulating symptom-related behaviors. Here, we contribute to the study of these variants through the generation and characterization of one such SCZ-associated risk gene, ZSWIM6. While no functional studies have been published on ZSWIM6, two independent genome-wide association studies have implicated it in SCZ[2,3] and several additional studies have documented its expression in developing and adult brain[4–7]. At least two clinical studies have also identified a recurrent point mutation in ZSWIM6 in cases of acromelic frontonasal dysostosis, a rare disorder characterized by multiple brain, limb, and craniofacial abnormalities including severe intellectual disability (ID)[7,8]. And while few of the known protein domains within ZSWIM6 are well-characterized, gene ontology studies suggest that ZSWIM6 may participate in the epigenetic regulation of gene transcription through interactions with chromatin remodeling complexes[9] — a process recently implicated in the pathogenesis of multiple neurodevelopmental disorders[10–15].

Recent evidence has implicated cortico-striato-thalamic circuit dysfunction in multiple neuropsychiatric diseases exhibiting motor and cognitive behavioral components[16,17], reflecting the wide-ranging function of these pathways in motor control, decision-making and reward processing. Here, through the generation of Zswim6 knockout (KO) mice, we provide evidence that further implicates striatal dysfunction in the pathophysiology of motor dysregulation. We show that Zswim6 initially exhibits widespread early embryonic expression in many forebrain regions but becomes progressively restricted to the adult striatum postnatally. Consistent with this highly restricted expression pattern, we observed that Zswim6 KO mice exhibit reduced dendritic complexity in striatal medium spiny neurons (MSN), and a range of motor abnormalities consistent with striatal dysfunction. These data suggest that Zswim6 KO mice may serve as an important genetic tool for studying not only SCZ-associated neural circuit pathology, but neural circuits related to other neurodevelopmental disorders such as autism spectrum disorders and ID.

RESULTS

Expression of Zswim6 in the developing and adult forebrain

To confirm previous reports[18] and to examine Zswim6 across forebrain development, Zswim6 expression was evaluated by mRNA in situ hybridization and quantitative PCR (qPCR). Zswim6 was detected in the subventricular zone (SVZ) of the ganglionic eminences at embryonic day (E) 12.5 (Fig. 1A–C). Higher expression levels appeared in the lateral ganglionic eminence (LGE) than in the medial ganglionic eminence (MGE; Fig. 1K). By E14.5 this expression remained enriched in the SVZ and marginal zones of the ganglionic eminences and could also be detected at low levels in the cortical plate, developing amygdala, and thalamus (Fig. 1D–F). By E16.5, Zswim6 expression increased in the cortical plate, developing amygdala, and portions of the thalamus and hypothalamus (Fig. 1G–I). In the telencephalon, the postnatal expression of Zswim6 became more restricted to the striatum (Fig. 1J). Similar expression patterns have been identified in human samples (Supp. Fig. 1). We also compared the relative expression levels of two Zswim6 paralogues, Zswim4 and Zswim5, using qPCR in the developing striatum (Fig. 1L). While Zswim4 levels downregulate over time, Zswim5 and Zswim6 levels increase slightly between E13.5 and post-natal day 0 (P0). Remarkably, between P0 and adult, Zswim5 is substantially downregulated while Zswim6 is maintained at levels similar to those detected embryonically (Fig. 1L).

Generation of a Zswim6 knockout mouse line

This expression pattern in neocortical and striatal areas, and the association of Zswim6 with several neurodevelopmental disorders led us to evaluate whether loss of Zswim6 would alter forebrain development and function. Gene targeting was used to create a knockout allele (Fig. 2A) in which exon 4 was flanked by LoxP sequences. Removal of exon 4 was predicted to result in a frameshift mutation. Southern blotting was used to identify correctly targeted embryonic stem cell clones (Fig. 2B). Crosses with a germline expressed Cre recombinase line (CMV-Cre) resulted in generation of an allele lacking expression of Zswim6 exon 4 as demonstrated by in situ hybridization and reverse transcription-PCR (RT-PCR; Fig. 2C, D). The MGE of homozygous mutants expressed Zswim6 transcript downstream of the deleted region at roughly 35% of control levels at E13.5 (Fig. 2E), consistent with significant nonsense-mediated transcript decay. Of note, in silico analysis and 5′ RACE experiments suggest that Zswim6 has a single transcript (not shown). While the loss of exon 4 transcript and striatal-related phenotypes presented in this paper are strongly suggestive of the creation of a null allele, we were unable to confirm Zswim6 protein expression using commercial or custom-made antibodies.

Abnormal neocortical and striatal development in Zswim6 knockout mice

Zswim6 KO mice were born in Mendelian ratios, but showed increased neonatal mortality such that roughly 40% of KO mice survived to weaning (Fig. 3A, B). At postnatal day (P) 21, their weight averaged about 80% of wild-type controls (Fig. 3C), although this improved to 93% of controls by adulthood (Fig. 3C). Analysis of overhead-view surface area in P80 adults showed a subtle but significant decrease for the Zswim6 KO cerebral cortex, and no such decrease for the cerebellum (Fig. 3D). Stereological analysis of cortical and striatal

volumes by the Cavalieri method at P80 showed a 7% decrease of cortical volume and a 15% decrease in striatal volume (Fig. 3D). To determine whether the reduction in striatal volume is present throughout development, we measured striatal volumes at P0 and P21. At P21, Zswim6 KO mice had a 15% reduction in striatal volume, similar to that seen in adults (Fig. 3D). At P0, we found a non-significant 7% reduction in striatal volume relative to wild-type controls (Fig. 3D).

To further explore these phenotypes, we conducted stereological counting of immune-labeled neuronal subtypes in the dorsal striatum (striatum dorsal to the nucleus accumbens) of adult mice. Relative to wild-type controls, Zswim6 KO mice showed a 17% reduction in the number of nuclei labeling with CTIP2, a marker of medium spiny neurons (Fig. 4A). However, the density of these neurons was not changed. In contrast, there was no change in the number of striatal interneurons (Fig. 4B), defined by parvalbumin (PV), somatostatin (SST) and choline acetyl-transferase immunoreactivity. There were no gross alterations in the expression of dopamine receptors DRD1 or DRD2 by in situ hybridization (not shown), and no gross change in tyrosine hydroxylase or DARPP32 (not shown). Finally, there were no statistically significant changes in expression of several striatal genes evaluated by qPCR (Fig. 4C), including GPR88, PENK, Adora2a, Drd1, Drd2, Rgs4, TAC1, and GPR6. It is important to note that while more subtle changes in the expression levels of these genes may be present, our study was only powered to detect effect sizes of 30% or greater.

In addition to neuronal number, another important component of striatal size is dendritic arborization[19]. Reconstructions of Golgi-stained neurons revealed a significant decrease in dendritic number, branch points or nodes, tips, and total length (Fig. 5A, C). There was no change in the mean dendritic length. Sholl analysis revealed that Zswim6 KO mice have reduced cumulative dendritic length and decreased Sholl intersections (Fig. 5B). Furthermore, spine density was reduced in the KOs by about 15% (Fig. 5D).

To evaluate potential mechanisms behind the reduction of striatal medium spiny neurons, we quantified markers of proliferation during embryonic development. Counts of the m-phase marker PH3, and the S-phase marker EdU, at E14.5 showed no differences in the LGE between Zswim6 KO embryos and wild-type controls (Supp. Fig. 2). In addition, there was no gross difference in the density of cells expressing cyclin-D2, expressed primarily in subventricular zone progenitors (not shown). While these analyses cannot definitively rule out the presence of a subtle proliferation deficit, they do suggest that the adult striatal phenotype in Zswim6 KO mice is not secondary to a major proliferation deficit. In addition, we also investigated the presence of cleaved caspase-3 as an indicator of apoptosis in Zswim6 KO and control mice at E14.5, P0, P21, and P60 and found no increase in its expression (not shown).

Loss of Zswim6 results in behavioral deficits

To determine whether the alterations in medium spiny neuron number and structure are accompanied by behavioral abnormalities in Zswim6 KOs, mice were subjected to tests of motor output, assaying both motor learning and motor control. Consistent with an alteration of striatal function, Zswim6 KO mice exhibited impaired learning on the accelerating rotarod, despite similar levels of initial coordination (Fig. 6A). Force plate mediated gait

analysis did not reveal changes in stride length, stride rate or velocity (Supp. Fig. 3A–C). In both IR-beam open-field testing and force plate actometry measurements, Zswim6 KO mice exhibit modest hyperactivity, with increases in total distance traveled and a decrease in the number of low mobility bouts (LMB) – defined as a temporal block of 5 seconds in which the mouse's center of gravity did not extend beyond a 30 mm circle (Figure 6B, C). To further explore behaviors occurring during these LMBs, we focused on grooming behaviors by identifying a unique power spectra profile for phase 4 grooming, marked by peaks at frequencies of 6 and 12Hz (Figure 6Di). During LMBs, mutant mice were more likely to be engaged in grooming behaviors than wildtype littermates (Figure 6Dii). Mutants also exhibited an increase in the consecutive repetition of grooming bouts, but no change in their overall vigor as measured by the peaks of the averaged power spectra (Fig. 6Diii, Div). Zswim6 KO mice also exhibited other repetitive motor outputs, including a significant increase in the number of rearing events and hind limb jumps performed at the sides of the cage (Figure 6B, C). Furthermore, mutant mice exhibited a significant absolute directional bias in their turning behaviors, measured over the course of the 60-minute session (Figure 6C). This phenotype has been observed both in mutant mice with striatal dysfunction and in C57-Bl6 strains given amphetamine to boost dopaminergic signaling[20,21].

To probe whether Zswim6 KO mice might have enhanced striatal dopamine signaling, we subjected them to a sub-threshold amphetamine challenge [22]. Remarkably amphetamine, at a dose (2mg/kg) that did not alter the activity of controls, significantly increased the locomotor activity of the Zswim6 KOs (Fig. 6E).

DISCUSSION

To our knowledge this is the first paper to describe a loss-of-function model of the schizophrenia- and intellectual disability-associated gene Zswim6 in mice. Zswim6 is strongly expressed within the subventricular and mantle zones of the striatal anlage. Broadly, it has a dynamic expression pattern in multiple regions, including the neocortex, medial habenula, and the amygdala. Due to the strong persistent expression of Zswim6 in the adult striatum, the lack of functionally redundant molecules in this region, and the relevance of striatal dysfunction to neuropsychiatric motor and cognitive abnormalities, we focused our analyses on striatal morphology and motor control behaviors.

Striatal volume was reduced by approximately 15% in both P21 and adult Zswim6 KO mice. Although we found a borderline (P=.09) non-significant 7% reduction of striatal volume at P0, it trends with the reduction of striatal volume found at later ages, suggesting that both pre- and postnatal processes may contribute to the loss of striatal volume. This occurred in part due to a reduction in the number of medium spiny neurons (Fig. 4). To examine the mechanism of reduced medium spiny neuron number, proliferation was examined in embryonic Zswim6 KOs. No gross change was found at E14.5 (Supp. Fig. 2), although a subtle proliferation defect could still result in the observed 15% change in striatal volume. In addition, there was no increase in the expression of the apoptosis marker cleaved caspase 3 at E14.5, P0, P21 or in adults (data not shown).

To determine whether striatal volume loss could be secondary to both cell reductions and to altered cellular morphology in the Zswim6 KOs, adults were subjected to Golgi-Cox staining (Fig. 5). Indeed, there was a significant reduction in total dendritic length and in the number of dendrites per cell. Spine density was also significantly decreased, suggesting a loss of synaptic input. Together these data suggest that dendritic arborization is broadly impaired, yielding medium spiny neurons with reduced dendritic fields - a key integrator of striatal synaptic activity[23] and the purported site of up-state generation[24]. While based on the expression patterns of Zswim6 and Zswim5 this is most likely cell autonomous, the issue warrants further investigation, for example, through analysis of glia, vasculature, and neurotrophic support from striatal afferents.

Based on the observed striatal morphological abnormalities, Zswim6 mice were examined in behavioral paradigms for motor learning and overall behavioral control. Mutants exhibited a deficit in rotarod learning (Fig. 6A) that could not be explained by altered initial coordination, or genotypic differences in stride length, rate or velocity (Supp. Fig. 3). Zswim6 mutant mice consistently displayed hyperactivity, as demonstrated by both an increased distance traveled and a decrease in the number of LMBs (Fig. 6B, C). When LMBs were examined in further detail, it became apparent that Zswim6 KO mice spent a larger proportion of this stationary time engaged in grooming. Furthermore, they were more likely to string together either multiple or extended duration grooming bouts, as measured by detection of phase 4 grooming power spectral fingerprints (Figure 6D). In addition to increased relative grooming frequency and repetitive grooming structure, mutant mice also exhibited increased rearing and hind limb jumping behavior (Figure 6B, C), consistent with broad disruptions to motor control. These data, together with the enhanced rotational bias observed in mutants may be suggestive of an enhanced dopaminergic signaling in the absence of Zswim6. In support of this hypothesis, the hyperactivity of Zswim6 KOs in the open field test was further increased by a dose of amphetamine that had no effect on the activity of wildtype littermate controls (Fig. 6E). Interestingly, Zswim6 has been shown to be expressed at higher levels in D2R-expressing striatopallidal MSN than in D1R-expressing striatonigral MSN[25]. Thus, loss of Zswim6 may preferentially impair the function of D2R+ MSN. Broadly speaking, this is consistent with our hyperactivity and amphetamine data, which suggest a bias toward D1R+ MSN activity and away from D2R+ MSN function. Although we currently lack definitive evidence, this is supported by studies showing that loss of D2R+ MSN of the dorsal striatum leads to enhanced responses to cocaine[26]. Taken together, these alterations are consistent with defects in striatal functioning and suggest that at baseline Zswim6 KO mice may have increased dopaminergic tone, an interesting topic for future studies.

A major question remaining to be addressed is how loss of Zswim6 results in striatal pathology. Zswim6, like its close paralogues Zswim4 and Zswim5, is a gene of unknown function. However, all three proteins contain the highly conserved zinc-finger-like SWIM domain, which is predicted to interact with either DNA or proteins in different contexts[9]. Interestingly, SWIM domains are found in certain types of bacterial SWI2/SNF2 ATPases, which function in chromatin remodeling[9]. Eukaryotic SWIM domain-containing proteins that no longer contain an ATPase domain are hypothesized to interact with eukaryotic chromatin-associated SWI2/SNF2 ATPases[9], although concrete evidence is currently

lacking. Additionally, Zswim6 has a third paralogue, Zswim8, whose function has been studied in *C. elegans*. Zswim8 (EBAX-1) serves as a substrate recognition subunit in the BC-box Cullin-RING E3 ligase (CRL) complex, which participates in protein quality control by targeting misfolded SAX-3/Robo to the proteasome[27]. Zswim6 also contains BC- and Cul2-boxes, suggesting that Zswim6 could similarly function as an E3 ubiquitin ligase (Supp. Fig. 4)[28]. Curiously, Zswim6 has been shown to interact with the E3 ubiquitin ligase HECW2[29]. Mutations in HECW2 were recently identified in patients with intellectual disability and epilepsy, some of whom also display abnormal, repetitive motor behaviors[30,31]. Further studies are necessary to understand whether, and if so how, Zswim6 participates in these diverse cellular processes.

In addition to its association with schizophrenia and educational attainment, a recurrent point mutation in ZSWIM6 has been identified in several human patients with acromelic frontonasal dysostosis[7,8]. This syndrome exhibits several features including hypertelorism, median facial cleft, and preaxial polydactyly. On a gross level, Zswim6 KO mice did not display any of these features, suggesting that the recurrent human mutation acts as a dominant gain-of-function rather than as a dominant negative.

In sum, we have generated KO mutant mice for the schizophrenia-associated gene Zswim6. Loss of Zswim6 results in striatal abnormalities that are consistent with previously described schizophrenia-associated endophenotypes, in particular the hypersensitivity to amphetamine. Additionally, since the targeting construct includes the capacity to generate conditional mutants, future studies will be able to evaluate whether postnatal loss of Zswim6 can recapitulate these constitutive KO phenotypes. We thus conclude that this targeted genetic mutation appears to be a useful mouse model for studying the functional contributions of Zswim6 to nervous system development and the growing number of disease states associated with it.

Materials and Methods

Mouse Lines

This study was carried out in strict accordance with the recommendations in the Guide for the Care and Use of Laboratory Animals of the National Institutes of Health. The protocol was approved by the Institutional Animal Care and Use Committee at The Children's Hospital of Philadelphia (Protocol Number: 2012-4-1004). ABR measurements were performed under anesthesia (ketamine (100mg/kg)/xylazine (10mg/kg) cocktail). Adult mice were euthanized by isoflurane overdose, followed by cervical dislocation. All efforts were made to minimize suffering. Behavioral experiments were performed during the first 3 hours of the light phase (7:00–11:00am) and animals were allowed to acclimate to the procedure room for at least 15 minutes before beginning experiments. Primers used for genotyping animals and for generating in situ hybridization probes are summarized in Table 1.

We worked with Ingenious Targeting Laboratories (Ronkonkoma, New York, USA) to make the Zswim6 knockout. A 13.75-kb Zswim6 genomic fragment was subcloned from a C57BL/6 BAC clone to construct the targeting vector using homologous recombination. A FRT-LoxP-Neo-FRT-LoxP cassette was inserted downstream of exon 4 and the third single

LoxP site was inserted upstream of exon 4. The region flanked by the second and third LoxP sites is approximately 569bp. Exon 4 encodes amino acids 337-386 and its deletion causes an early stop. The short homology arm extends 2.1kb to the 3′ end of the FRT-LoxP-Neo-FRT-LoxP cassette, whereas the long homology arm extends 5.1kb from the 5′ side of the third LoxP site. The linearized targeting vector was then electroporated into iTL BA1(C57BL/6X129/SvEv) hybrid embryonic stem cells.

Targeted embryonic stem cells were microinjected into C57BL/6 blastocysts. Resulting chimeras with a high percentage agouti coat color were mated to C57BL/6 FLP mice to remove the Neo cassette. Heterozygous mice confirmed for somatic neo deletion were then bred to wild type C57 mice to remove the FLP transgene. To generate germline KO alleles, Zswim6$^{+/F}$ mice were bred to CMV-cre delete mice (The Jackson Laboratory Stock NO: 006054) to generate Zswim6$^{+/-}$ animals.

Tissue Preparation for Immunohistochemistry

Following euthanasia with isoflurane, mice were perfused with 4% paraformaldehyde (PFA) in PBS and post-fixed in 4% PFA overnight. Brains were then embedded in 4% low-melting-point agarose, cut in 50μm sections with a vibrating microtome (Leica), and stored in antifreeze solution (30% ethylene glycol and 30% glycerol in 1x PBS) at −20°C until processing. For embryonic samples, embryos were fixed overnight at 4°C in RNase-free 4% PFA in 1x PBS. Embryos were then washed two times in 1x PBS and cryoprotected by immersion through sucrose (15 and 30% sucrose in 1x PBS; solutions were changed once embryos had sunk). Afterwards they were embedded in freezing compound and stored at −80°C until sectioning.

Immunohistochemistry

Brain sections were pre-incubated for one hour in blocking buffer (5% bovine serum albumin with 0.1% Triton-X-100). Sections were then incubated overnight at 4°C with the following primary antibodies: rabbit anti-PV (Swant, PV-25; 1:2000), rat anti-SST (Millipore, 14224; 1:200), rat anti-CTIP2 (Abcam, ab18465, 1:500), goat anti-ChAT (Chemicon, ab144P, 1:200), rabbit anti-phospho-Histone H3 (Millipore, 06-570, 1:400), rabbit anti-cyclinD2 (Santa Cruz, M-20, 1:5000), rabbit anti-DARPP32 (Abcam, ab40801, 1:1000), mouse anti-TH (Millipore, MAB318, 1:200). Secondary antibodies were conjugated to Alexa fluorophores (488, 568 or 680, Invitrogen). DAPI (300nM) was applied concurrently with secondary antibodies to label cell nuclei. EdU signals were detected with the Click-iT EdU Alexa Fluor 647 imaging kit (Invitrogen, Carlsbad, CA, USA).

Cell Counting

Stereological analysis for CTIP2 was conducted on a Nikon E600 microscope equipped with a motorized stage and Stereoinvestigator software (MicroBrightField). CTIP2 cell counts were obtained using the Optical Fractionator Probe and systematic random sampling at 40x magnification. Optical dissector frame and counting grid sizes of 60μm × 60μm and 700μm × 700μm, respectively, were used. Striatal contours were delineated as described by Franklin and Paxinos (2008). Starting from the genu of the corpus callosum, every 5th section was evaluated for a total of 6 sections.

For PV, SST, and ChAT cell counts, 10x montages of entire brain sections were generated using Stereoinvestigator's Virtual Tissue module. Starting from the genu of the corpus callosum, every 5th section was imaged for a total of 6 sections. Images were opened using ImageJ and the striatum was delineated as described by Franklin and Paxinos (2008). Using the ImageJ cell counter plugin, striatal interneurons from each brain section were counted and then summated. Statistical significance was determined using a two-tailed Student's t-test. Littermate controls were used for this analysis.

For PH3 and EdU counts, image stacks were opened in ImageJ and three 120μm × 120μm boxes were drawn beginning at the apical surface and extending outward from the LGE along a line that was approximately equidistant from the pallial-subpallial angle and MGE-LGE sulcus (as shown in supplemental figure 2). This analysis required the use of littermate embryos from two distinct litters.

Volumetric Analyses and Surface Area

Volumetric analyses were done using the Cavalieri estimator on Stereoinvestigator (MicroBrightField). We used a total of 11, 50μm-thick sections in our analysis, where section 3 of 11 along the rostrocaudal axis corresponded to the first section in which the genu of the corpus callosum could be identified, and used every 5th section from that point. Cortical contours were drawn using the pial surface as the outside boundary and terminated laterally at a point that was perpendicular to the midline. For surface area analyses, we took overhead images of adult brains using a dissection microscope fitted with a digital camera. Images were then opened in ImageJ and analyzed using the area measure tool. Statistical significance for volumetric and surface area analyses were determined using a two-tailed Student's t-test. Adult volumetric and surface area analyses were performed on littermate controls from a total of 3 distinct litters. For P21 and P0 striatal volume measurements, littermate controls from 2 and 3 distinct litters were used, respectively.

Quantitative PCR (qPCR) Analysis

Following euthanasia with isoflurane, Zswim6 mice were decapitated and their brains rapidly dissected. Brains were then sectioned at 400μm in ice-cold PBS using a vibrating microtome. Dorsal striatum was carefully dissected and placed in TRIzol reagent (Invitrogen) for RNA extraction using the PureLink RNA Mini kit (Invitrogen). cDNA was synthesized using the VILO cDNA synthesis kit (Invitrogen). qPCR was conducted using Taqman Gene Expression Assays (Applied Biosystems). Each sample was run in triplicate, along with probes for GAPDH on the same plate, on a Stratagene MX3005P real-time PCR machine (La Jolla, CA) following the manufacturer's recommended protocol. Littermate controls from 2 distinct litters were used in this analysis. Data were analyzed using the comparative C_T method. Statistical significance was determined using a two-tailed Student's t-test.

Golgi-Cox Staining and Neuron Reconstruction

Golgi-Cox staining was performed using the FD Rapid GolgiStain kit (FD NeuroTechnologies). Brains were incubated in a potassium dichromate solution for 2 weeks in the dark, then with silver nitrate for another two days before being cut into 150μm

sections with a vibrating microtome (Leica). Golgi staining was then performed on slides. Cell bodies and dendrites of striatal medium spiny neurons (MSN) from each group were traced and analyzed using Neurolucida (MicroBrightField). Only MSN within the dorsal striatum were traced. Littermate controls from 2 distinct litters were used for this analysis. Morphological differences were analyzed using a one-tailed Student's t-test. For Sholl analyses, a two-way ANOVA was used to determine significance using Prism 5 (GraphPad). A total of 30 MSN were traced from each group (10 neurons per brain, 3 brains per group).

Spine Density Analysis

For spine quantification, dendrites were traced using Neurolucida (MicroBrightField) and divided into 10μm segments using a 100x oil-immersion objective. For each analysis, we counted spines from a minimum of 10 neurons from each animal. For MSN, we counted spine density at a distance of 60–150μm from the soma and analyzed a minimum of 40μm from each neuron; both primary and secondary dendrites were included. A total of 2400μm of dendrite were analyzed from each group and the reported average is the spine density for each group between 60–150μm. Statistical significance was determined using a one-tailed Student's t-test, where each data point represented the average number of spines per 10μm for the dendritic range (e.g. 60–150μm for MSN) that we analyzed.

In Situ RNA Hybridization

We generated cDNA templates for riboprobe synthesis for Zswim5 and Zswim6 by nested PCR incorporation of T7 and Sp6 RNA polymerase promoters using the primers listed in Table 1. Template cDNA was obtained from E13.5 mouse brain. cDNA plasmids for DRD1 and DRD2 were gifts from Kenneth Campbell. On the day of in situ hybridization, adult sections were mounted onto Superfrost Plus slides (Fisher Scientific, Pittsburgh, PA) and allowed to dry at room temperature for 2 hours before processing. Following incubation in prehybridization buffer for 2 hours at 60°C, sections were incubated with digoxigenin-labeled riboprobes for 16 hours at 58°C. After rinsing, sections were incubated with an alkaline phosphatase-conjugated sheep anti-digoxigenin antibody (Roche, 1:2000) in blocking buffer at 4°C for 16 hours and developed in nitroblue tetrazolium/5-bromo-4-chloro-3-indolyl phosphate solution (7μl/ml in 10% polyvinyl alcohol; Roche) in the dark for 12–48 hours. Fresh developing solution was exchanged every 24 hours. After developing, material was rinsed, and alkaline phosphatase activity was quenched by fixation in 4% PFA containing 0.125% glutaraldehyde. Sections were then rinsed, cleared in 50% glycerol in 1x PBS, and mounted using aqueous mounting media.

Rotarod

For high speed rotarod performance testing a five-station Rotarod treadmill (IITC) was used. Rotarod testing consisted of three trials per day over the course of 4 days. Days 1 and 2 consisted of 4–40rpm trials over a 300 second period with a constant rate of acceleration. Days 3 and 4 consisted of 8–80rpm trials over a 300 second period. A trial was terminated when a mouse fell off, made one complete backward revolution while hanging on, or after 300 seconds (maximum speed, no further acceleration). On day 1, mice were allowed to acclimate to the rod for 1 minute before beginning the first trial. On each testing day, mice were left in the room for 15 minutes to acclimate before testing. The machine was wiped

down with 70% ethanol in between each trial. In order to compare mice of similar age, two separate cohorts of approximately 7 to 8 mice per group were tested. Littermate controls from an average of 4 distinct litters were used for each cohort. As performance on the rotarod for both time to failure and terminal speed was not normally distributed by group (Shapiro-Wilk test, $p<0.001$), differences between Zswim6 KO mice and controls were analyzed non-parametrically with a Mann-Whitney U test.

Open Field

Locomotor activity was assessed with the automated Photobeam Activity System (San Diego Instruments). After acclimating to the room for 15 minutes, mice were individually placed in a 16 × 16 inch arena outfitted with photocells to detect horizontal and rearing activities over the course of 10 minutes. The 10-minute trial began as soon as the mouse was placed into the arena. The arena was cleaned with 70% ethanol in between mice. Control and mutant mice for the 10-minute open field test were compared using a one-tailed Student's t test (unpaired). For amphetamine-sensitivity testing, mice were placed in the open field arena for 30 minutes before being injected with either a 2 mg/kg D-amphetamine hemisulfate salt (Sigma) solution prepared in isotonic saline at a concentration of 0.2 mg/ml or isotonic saline as control. Immediately after injection, mice were placed back into the arena for an additional 1 hour. Response to amphetamine in the open field experiments was analyzed via longitudinal mixed-effects regression clustering on individual mice. The same cohort of wildtype and mutant mice was used for the 10-minute open field, amphetamine challenge, and rotarod experiments. Mice were first subjected to the 10-minute open field challenge. After a 2 week rest period, the mice were tested on the rotarod. After an additional 6 week rest period, the mice were subjected to amphetamine testing.

Force Plate Actometer

Force-plate actometer assays were performed using approaches previously described[21,32]. Each trial was 60 minutes in length. The signals from the 4 transducers (sampled at 200 scans/s) were summed (this sum results in Fz, the vertical ground reaction force). Next, Fz values were expressed as a percentage of body weight to control for differences in body weight. The Fz time series data were then multiplied in MATLAB by the Hanning data window, which acts to minimize discrete Fourier transform "leakage" associated with the start and end of digitized time series. The fft function in MATLAB was used to calculate the fast Fourier transformation of raw Fz data. The resulting data matrix of power spectra was written to a text file that was read by SYSTAT for further manipulation. To unambiguously identify phase 4 grooming events, mice were filmed during force plate recordings and grooming bouts were evoked by water misting on the whiskers of the mice. By convention, grooming may only take place during low mobility bouts, which are mutually exclusive from the rest of the run, when mice are either ambulating or climbing. Littermate controls from 5 distinct litters were used in this analysis.

Supplementary Material

Refer to Web version on PubMed Central for supplementary material.

Acknowledgments

We thank William (Tim) O'Brien at the University of Pennsylvania Neurobehavior Testing Core who is partially supported by the Preclinical Models Core of the Intellectual and Developmental Disabilities at CHOP/Penn (U54 HD086984) for his help with the behavioral analyses. We also thank Ivor Asztalos for help with statistical analyses. This work was supported by an NIH R01 MH066912 (S.A.A) and F30 MH105045-02 (D.J.T).

References

1. McCarroll SA, Hyman SE. Progress in the genetics of polygenic brain disorders: significant new challenges for neurobiology. Neuron. 2013; 80:578–587. DOI: 10.1016/j.neuron.2013.10.046 [PubMed: 24183011]
2. Schizophrenia Working Group of the Psychiatric Genomics C. Biological insights from 108 schizophrenia-associated genetic loci. Nature. 2014; 511:421–427. DOI: 10.1038/nature13595 [PubMed: 25056061]
3. Ripke S, et al. Genome-wide association analysis identifies 13 new risk loci for schizophrenia. Nature genetics. 2013; 45:1150–1159. DOI: 10.1038/ng.2742 [PubMed: 23974872]
4. Atlas, AB. Allen Instutite for Brain Science. 2012. <http://www.alleninstitute.org>
5. Visel A, Thaller C, Eichele G. GenePaint.org: an atlas of gene expression patterns in the mouse embryo. Nucleic Acids Res. 2004; 32:D552–556. DOI: 10.1093/nar/gkh029 [PubMed: 14681479]
6. Blackshaw S, et al. Molecular pathways controlling development of thalamus and hypothalamus: from neural specification to circuit formation. The Journal of neuroscience: the official journal of the Society for Neuroscience. 2010; 30:14925–14930. DOI: 10.1523/JNEUROSCI.4499-10.2010 [PubMed: 21068293]
7. Smith JD, et al. Exome sequencing identifies a recurrent de novo ZSWIM6 mutation associated with acromelic frontonasal dysostosis. Am J Hum Genet. 2014; 95:235–240. DOI: 10.1016/j.ajhg.2014.07.008 [PubMed: 25105228]
8. Twigg SR, et al. Acromelic frontonasal dysostosis and ZSWIM6 mutation: phenotypic spectrum and mosaicism. Clin Genet. 2015
9. Makarova KS, Aravind L, Koonin EV. SWIM, a novel Zn-chelating domain present in bacteria, archaea and eukaryotes. Trends in biochemical sciences. 2002; 27:384–386. [PubMed: 12151216]
10. Ronan JL, Wu W, Crabtree GR. From neural development to cognition: unexpected roles for chromatin. Nat Rev Genet. 2013; 14:347–359. DOI: 10.1038/nrg3413 [PubMed: 23568486]
11. Koga M, et al. Involvement of SMARCA2/BRM in the SWI/SNF chromatin-remodeling complex in schizophrenia. Human molecular genetics. 2009; 18:2483–2494. DOI: 10.1093/hmg/ddp166 [PubMed: 19363039]
12. McCarthy SE, et al. De novo mutations in schizophrenia implicate chromatin remodeling and support a genetic overlap with autism and intellectual disability. Mol Psychiatry. 2014; 19:652–658. DOI: 10.1038/mp.2014.29 [PubMed: 24776741]
13. Krumm N, O'Roak BJ, Shendure J, Eichler EE. A de novo convergence of autism genetics and molecular neuroscience. Trends Neurosci. 2014; 37:95–105. DOI: 10.1016/j.tins.2013.11.005 [PubMed: 24387789]
14. Zhubi A, Cook EH, Guidotti A, Grayson DR. Epigenetic mechanisms in autism spectrum disorder. Int Rev Neurobiol. 2014; 115:203–244. DOI: 10.1016/B978-0-12-801311-3.00006-8 [PubMed: 25131546]
15. Rangasamy S, D'Mello SR, Narayanan V. Epigenetics, autism spectrum, and neurodevelopmental disorders. Neurotherapeutics. 2013; 10:742–756. DOI: 10.1007/s13311-013-0227-0 [PubMed: 24104594]
16. Fuccillo MV. Striatal Circuits as a Common Node for Autism Pathophysiology. Front Neurosci. 2016; 10:27. [PubMed: 26903795]
17. Shepherd GM. Corticostriatal connectivity and its role in disease. Nature reviews. Neuroscience. 2013; 14:278–291. DOI: 10.1038/nrn3469 [PubMed: 23511908]
18. Tucker ES, et al. Molecular specification and patterning of progenitor cells in the lateral and medial ganglionic eminences. The Journal of neuroscience: the official journal of the Society for

Neuroscience. 2008; 28:9504–9518. DOI: 10.1523/JNEUROSCI.2341-08.2008 [PubMed: 18799682]

19. Cazorla M, Shegda M, Ramesh B, Harrison NL, Kellendonk C. Striatal D2 receptors regulate dendritic morphology of medium spiny neurons via Kir2 channels. The Journal of neuroscience: the official journal of the Society for Neuroscience. 2012; 32:2398–2409. DOI: 10.1523/JNEUROSCI.6056-11.2012 [PubMed: 22396414]
20. Rothwell PE, et al. Autism-associated neuroligin-3 mutations commonly impair striatal circuits to boost repetitive behaviors. Cell. 2014; 158:198–212. DOI: 10.1016/j.cell.2014.04.045 [PubMed: 24995986]
21. Fowler SC, et al. A force-plate actometer for quantitating rodent behaviors: illustrative data on locomotion, rotation, spatial patterning, stereotypies, and tremor. J Neurosci Methods. 2001; 107:107–124. [PubMed: 11389948]
22. Gilani AI, et al. Interneuron precursor transplants in adult hippocampus reverse psychosis-relevant features in a mouse model of hippocampal disinhibition. Proceedings of the National Academy of Sciences of the United States of America. 2014; 111:7450–7455. DOI: 10.1073/pnas.1316488111 [PubMed: 24794528]
23. Carter AG, Sabatini BL. State-dependent calcium signaling in dendritic spines of striatal medium spiny neurons. Neuron. 2004; 44:483–493. DOI: 10.1016/j.neuron.2004.10.013 [PubMed: 15504328]
24. Plotkin JL, Day M, Surmeier DJ. Synaptically driven state transitions in distal dendrites of striatal spiny neurons. Nat Neurosci. 2011; 14:881–888. DOI: 10.1038/nn.2848 [PubMed: 21666674]
25. Lobo MK, Karsten SL, Gray M, Geschwind DH, Yang XW. FACS-array profiling of striatal projection neuron subtypes in juvenile and adult mouse brains. Nat Neurosci. 2006; 9:443–452. DOI: 10.1038/nn1654 [PubMed: 16491081]
26. Durieux PF, Schiffmann SN, de Kerchove d'Exaerde A. Differential regulation of motor control and response to dopaminergic drugs by D1R and D2R neurons in distinct dorsal striatum subregions. EMBO J. 2012; 31:640–653. DOI: 10.1038/emboj.2011.400 [PubMed: 22068054]
27. Wang Z, et al. The EBAX-type Cullin-RING E3 ligase and Hsp90 guard the protein quality of the SAX-3/Robo receptor in developing neurons. Neuron. 2013; 79:903–916. DOI: 10.1016/j.neuron.2013.06.035 [PubMed: 24012004]
28. Mahrour N, et al. Characterization of Cullin-box sequences that direct recruitment of Cul2-Rbx1 and Cul5-Rbx2 modules to Elongin BC-based ubiquitin ligases. J Biol Chem. 2008; 283:8005–8013. DOI: 10.1074/jbc.M706987200 [PubMed: 18187417]
29. Lu L, et al. The HECT type ubiquitin ligase NEDL2 is degraded by anaphase-promoting complex/cyclosome (APC/C)-Cdh1, and its tight regulation maintains the metaphase to anaphase transition. J Biol Chem. 2013; 288:35637–35650. DOI: 10.1074/jbc.M113.472076 [PubMed: 24163370]
30. Halvardson J, et al. Mutations in HECW2 are associated with intellectual disability and epilepsy. J Med Genet. 2016; 53:697–704. DOI: 10.1136/jmedgenet-2016-103814 [PubMed: 27334371]
31. Berko ER, et al. De novo missense variants in HECW2 are associated with neurodevelopmental delay and hypotonia. J Med Genet. 2016
32. McKerchar TL, Zarcone TJ, Fowler SC. Use of a force-plate actometer for detecting and quantifying vertical leaping induced by amphetamine in BALB/cJ mice, but not in C57BL/6J, DBA/2J, 129X1/SvJ, C3H/HeJ, and CD-1 mice. J Neurosci Methods. 2006; 153:48–54. DOI: 10.1016/j.jneumeth.2005.10.002 [PubMed: 16290200]

Highlights

- ZSWIM6 is associated with multiple neurodevelopmental disorders
- We report the initial generation and characterization of Zswim6 knockout (KO) mice
- Zswim6 KO mice have reductions in striatal volume and changes in MSN morphology
- Zswim6 KO mice display multiple abnormalities in motor control behaviors

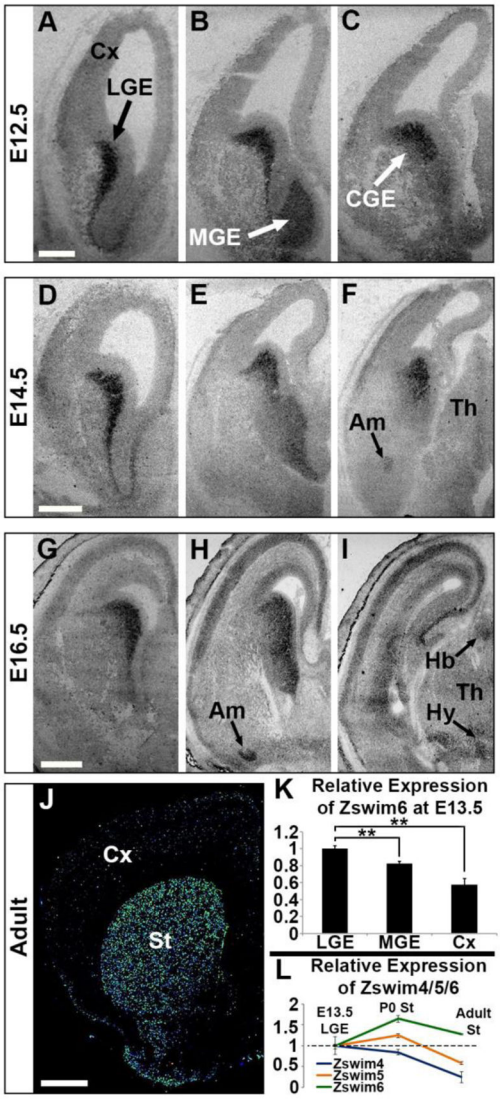

Fig. 1. Zswim6 expression during striatal development

At embryonic day (E) 12.5 (A–C) and E14.5 (D–F) Zswim6 mRNA is strongly expressed in the subventricular zone of the lateral, medial and caudal ganglionic eminences but at low to undetectable levels in the cerebral cortex. Low-level expression is also seen in the amygdala (arrow in F) and thalamus (G–I). At E16.5 this expression expands to the cortical plate and medial habenula (arrow in I) and increases in intensity in the amygdala (arrow in H). (J) Image from the Allen Brain Atlas shows that expression of Zswim6 is present in the adult striatum but not in the overlying cerebral cortex. (K) Quantitative PCR (qPCR) shows that Zswim6 is expressed at higher levels in the LGE than in the MGE or cortex at E13.5 (N=3 mice for each region). (L) qPCR for Zswim4, Zswim5, and Zswim6 across striatal development shows that while Zswim4 and Zswim5 are largely downregulated by adulthood, Zswim6 expression is maintained (N=3 mice for each region). Abbreviations: LGE (lateral ganglionic eminence); MGE (medial ganglionic eminence); CGE (caudal ganglionic eminence); Cx (cortex); Th (thalamus); Am (amygdala); Hb (habenula); Hy

(hypothalamus); St (striatum). Scale bars 300μm in A–C, 400μm in D–F, 500μm in G–I, 1000μm in J. ** p<.01. Error bars indicate SEM.

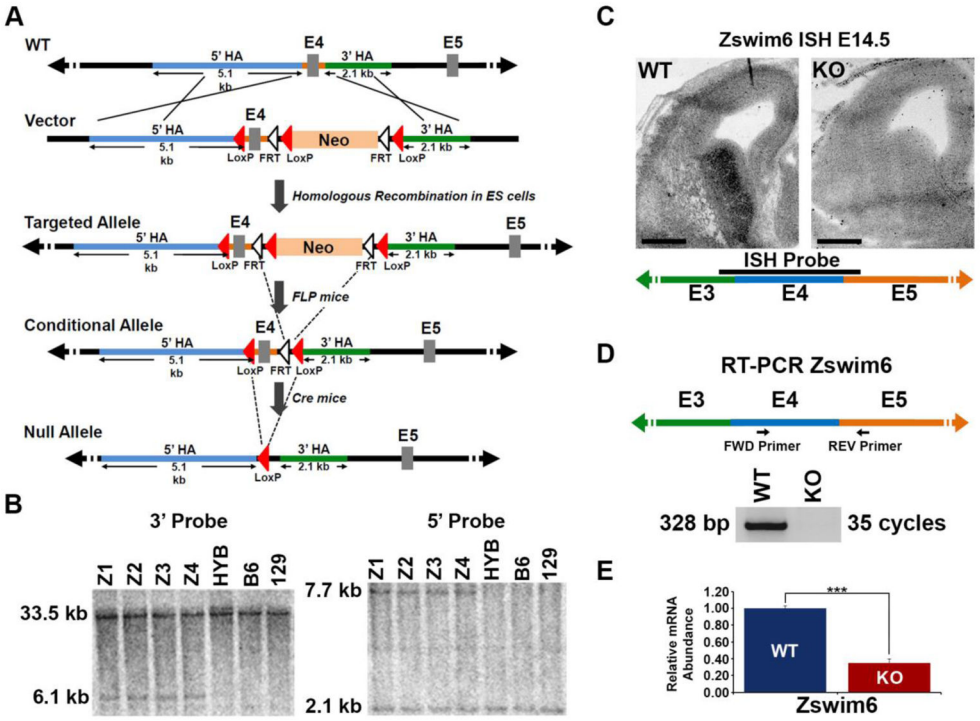

Fig. 2. Generation of Zswim6 knockout mice

(A) Schema of constructs used in generating a knockout (KO) allele for Zswim6 by flanking exon 4 with LoxP insertions, generating a mouse line, then crossing this line with Cre-deleter mice. (B) Southern blot analysis to identify correctly targeted embryonic stem (ES) cell clones obtained from hybrid C57BL/6x129/SvEv ES cells electroporated with the targeting construct. Four ES clones (Z1–Z4) were identified in which there were the expected 5′ and 3′ recombinations. HYB, hybrid ES cell; B6, C57BL/6 ES cell; 129, 129/SvEv ES cell. (C) In situ hybridization (ISH) for Zswim6 using a probe spanning from exon 3 to the beginning of exon 5 shows loss of expression in coronal sections from embryonic day (E) 14.5 forebrain of homozygous Zswim6 KOs. (D) RT-PCR reveals a loss of product created by primers flanking the exon 4 and 5 junction in the Zswim6 KO. (E) qPCR using a primer pair downstream from the deleted exon shows that there is a significant reduction in the relative abundance of Zswim6 mRNA in the MGE of E13.5 homozygous Zswim6 KO mice (N=3 mice). Abbreviations: WT (wild type); Neo (neomycin resistance cassette); E (exon). ***p<.001. Scale bar 400μm in C. Error bars indicate SEM.

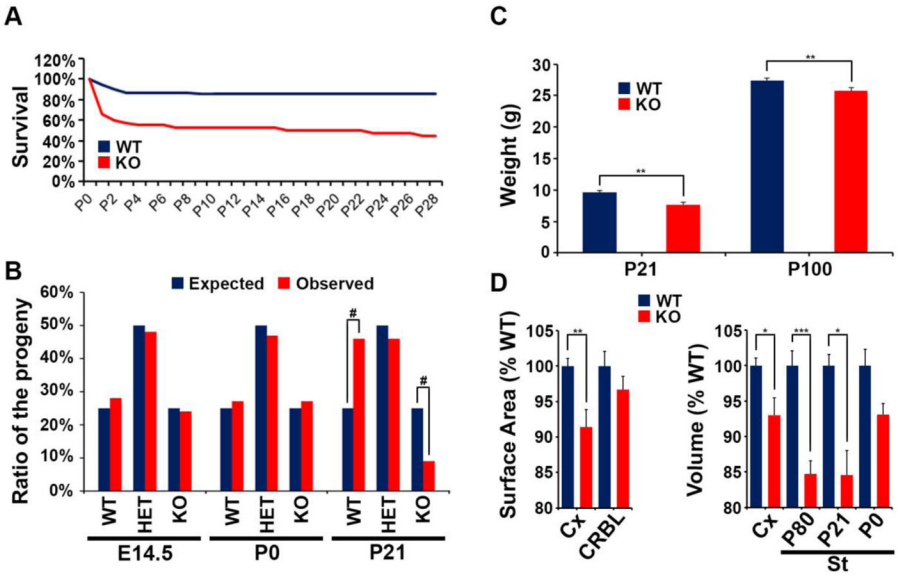

Fig. 3. Decreased early postnatal survival and forebrain size in Zswim6 KOs

(A) Survival plot showing that the Zswim6 KO mice have a 40% mortality in the first few days after birth, followed by a very gradual decline through 4 weeks. Data is from approximately 100 mice from each group. (B) Analysis of the % of litters that are wild type (WT), heterozygous (HET) or KO for Zswim6 at embryonic day (E) 14.5, post-natal day (P) 0, and P21 is consistent with loss of KO pups after birth. (N=79 mice for P21, X^2 (2) = 27.911) (C) Zswim6 KOs also show a small decrease of weight relative to controls at P21 that persists into adulthood (N=10 mice). (D) Overhead surface area of the cerebral cortex (Cx) at P80 shows a significant decrease in the Zswim6 KOs, but no change in the cerebellum (CRBL; N=5 brains). Volumetric measurements based on analysis of coronal tissue sections show a significant reduction of volume in both the Cx (N=5 WT, 6 KO brains) and the striatum (St) at P80 (N=5 brains), as well as in the striatum at P21 (N=4 brains), with a borderline non-significant reduction at P0 (N=5 brains). *p<.05, ** p<.01, ***p<.001, #p<.0001. Error bars indicate SEM.

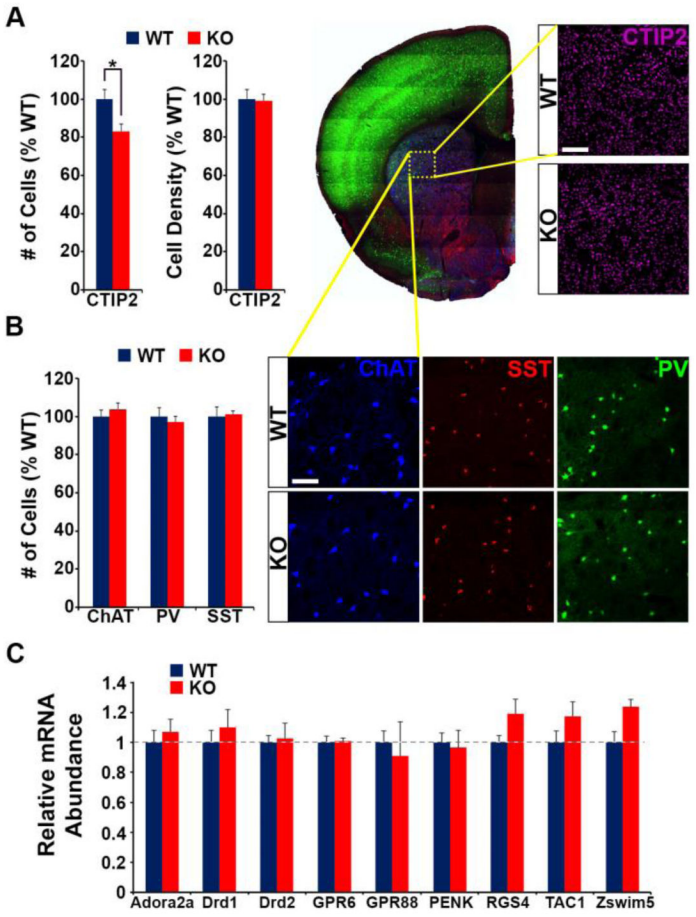

Fig. 4. Zswim6 knockouts have a reduced number of medium spiny neurons

(A) Cell counts for the medium spiny neuron marker CTIP2 in adult Zswim6 KOs relative to WT controls shows a significant reduction of cell number in the KOs. On the other hand cell density is unchanged, consistent with cell loss combined with reduced neuropil (i.e. total dendritic length; see Fig. 5). Representative immunostaining for CTIP2 is shown on the far right, from a region of striatum indicated by the dotted yellow box. (B) In contrast to the effects on medium spiny neurons, cell counts for several populations of striatal interneurons (choline acetyl transferase, ChAT; parvalbumin, PV; somatostatin, SST) are unchanged (N=3 brains). Representative immunostaining for ChAT, SST, and PV are shown to the right, from the same region of striatum indicated by the dotted yellow box shown above in Fig. 4A. (C) Semi-quantitative RT-PCR for striatal transcripts (shown relative to control values), including the dopamine receptors Drd1 and Drd2, are not altered in the Zswim6 KOs (N=3 mice). *p<.05. Scale bars 75μm in A and B. Error bars indicate SEM.

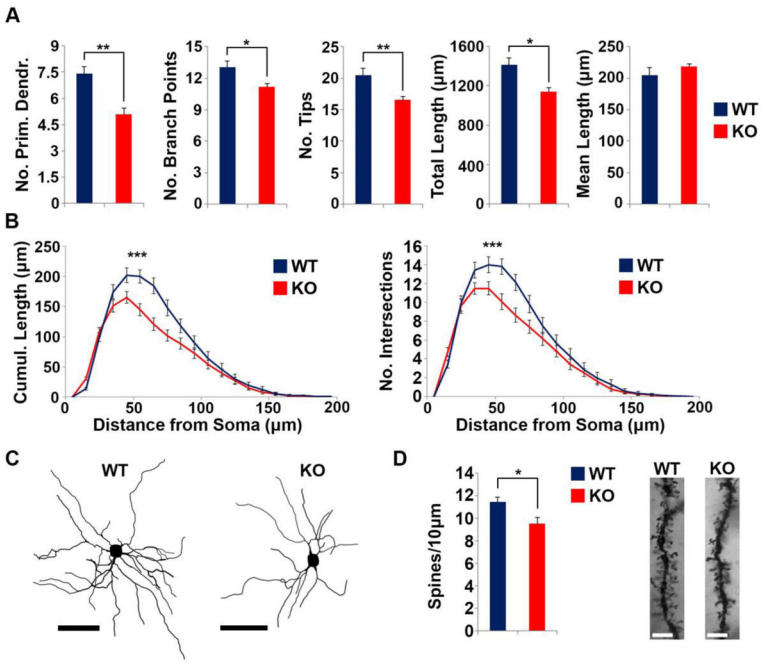

Fig. 5. Dendritic abnormalities in striatal medium spiny neurons of Zswim6 knockouts

(A) The number of primary dendrites, dendritic branch points or nodes, dendritic ends, and total length are decreased in the KOs, whereas there is no difference in mean length. (B) Consistent with the results in (A), Sholl analysis reveals decreased cumulative length and number of intersections in the KOs. (C) Shows an example of the reconstructions from Golgi-stained sections used in these analyses. (D) Spine density is also decreased on the medium spiny neurons of Zswim6 KOs (N=3 brains per group for all Golgi analyses). Scale bars 50µm in C, 5µm in D. *p<.05, ** p<.01, ***p<.001. Error bars indicate SEM.

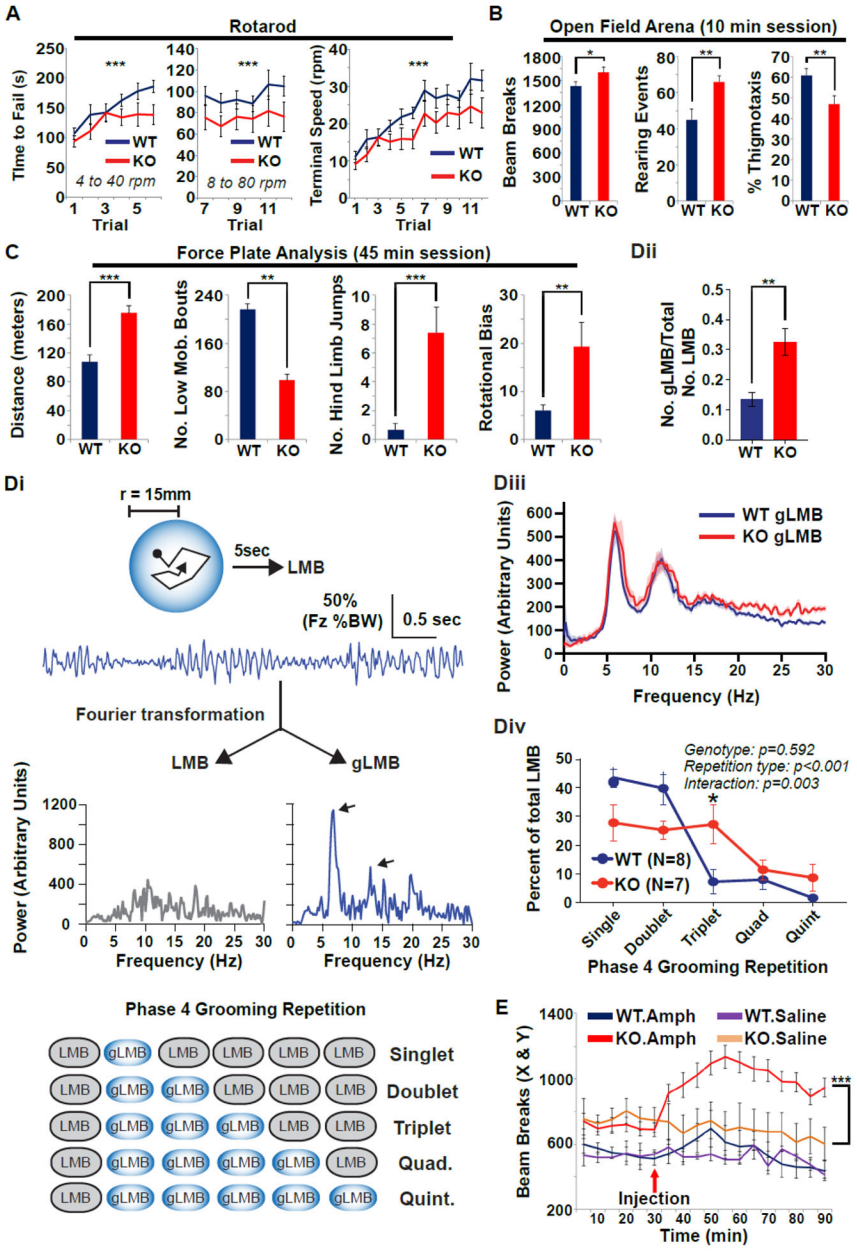

Fig. 6. Behavioral defects in Zswim6 knockout mice

(A) Zswim6 KOs achieve significantly lower terminal speeds and shorter times to fail (defined as falling off or making one complete backward revolution while holding on) on the rotarod test (N=14 WT, 15 KO mice). (B) In the open field the KOs have more beam breaks, more rearing events, and decreased thigmotaxis (N=16 WT, 19 KO mice). (C) Force plate analysis shows greater distance traveled, decreased low mobility bouts, increased hind limb jumps, and a significant absolute directional bias in the turning behaviors of Zswim6 KO mice referenced to the center of the actometer floor (N=9 WT, 7 KO mice). (Di) Schematic illustrating use of the force plate actometer to quantitatively measure grooming events. (Top) Low mobility bouts (LMBs) are defined as 5-second blocks where the center of gravity does

not extend beyond a circle with 15mm radius. (Middle) Fast Fourier transform yields a characteristic power spectra associated with phase 4 grooming (marked by peaks at ~6Hz and 12Hz, see arrowheads). (Bottom) Nomenclature for the pattern of phase 4 grooming events. (Dii) Mutant mice spend a greater fraction of LMBs grooming but do not show alterations in the power of these grooming events (Diii). (Div) Mutant mice exhibit a shift towards greater repetitions of phase 4 grooming, as defined in Di. (E) Amphetamine (2mg/kg; administered at 30 minutes) does not alter motility of controls (dark blue and purple lines show wild-types treated with amphetamine or saline, respectively; N=12 WT-amph, 13 KO-amph, 4 WT-saline, 4 KO-saline mice per group). In contrast, 2mg/kg amphetamine significantly increases the motility of the Zswim6 KOs over their moderately elevated baseline. *p<.05, **p<.01, ***p<.001. Error bars indicate SEM.

Table 1

Primers used for genotyping animals and generating in situ hybridization probes.

Mouse lines	Primer Name	Sequence	Floxed Allele	WT Allele	KO or Cre Allele	Purpose
Zswim6	Z6-3G-FWD	catggaagtacttgggtccga	893	716	~300	Genotyping
	Z6-3G-REV	ttctccatgtgggaaaactagaaag	893	716	~300	Genotyping
	DelExonP1-F	TGGCCATCAGCTTTGATCGT		328	no band	Confirm KO
	DelExonP1-R	TCGTCAATACTAGCACCCGC		328	no band	Confirm KO
	3′UTR_ISH-F	tacattacgcctttgcagtg		524		ISH
	3′UTR_ISH-R	ACATGAGTGAAGAAGTACAACC		524		ISH
	Exon3-5_F	GCAAGCCAGAGCAGGTCAAAC		478		ISH
	Exon3-5_R	TCATCCCAGAGCTGCCTATACTTG		478		ISH